Cellular automata model for citrus variegated chlorosis

M. L. Martins, G. Ceotto, S. G. Alves, C. C. B. Bufon, and J. M. Silva
Departamento de Física, Universidade Federal de Viçosa, 36571-000, Viçosa, Brazil

F. F. Laranjeira
Instituto Agronômico de Campinas, 13001-970, Campinas, Brazil
(Received 14 June 2000)

A cellular automata model is proposed to analyze the progress of citrus variegated chlorosis epidemics in São Paulo orange plantations. In this model epidemiological and environmental features, such as motility of sharpshooter vectors that perform Lévy flights, level of plant hydric and nutritional stress, and seasonal climatic effects, are included. The observed epidemic data were quantitatively reproduced by the proposed model on varying the parameters controlling vector motility, plant stress, and initial population of diseased plants.

PACS number(s): 87.10.+e, 87.19.Xx, 87.23.Cc

I. INTRODUCTION

Citrus variegated chlorosis (CVC) is an economically relevant disease affecting citrus [1]. In the São Paulo region (Brazil), one of the important citrus growing areas of the world, responsible for about 30% of the world production, CVC reduces the size and number of fruits by more than 35% [2]. CVC is considered to be potentially the most devastating citrus disease and represents the main threat to the Brazilian citrus industry, with annual revenues of the order of 1.2 to 1.4 billions of dollars. The losses associated with the disease are estimated at about 100 million dollars yearly [1].

CVC is caused by a xylem-limited bacterium, *Xyllela fastidiosa* [3], transmitted by xylem feeding, suctorial sharpshooter leafhoppers (Hemiptera: Cicadellidae) [4,5]. In São Paulo, the species *Dilobopterus costalimai* appears to be the most efficient vector for CVC transmission [5]. At present, a sweet orange cultivar resistant to *X. fastidiosa* is unknown, and control practices for CVC (bactericidal agents, systematic pruning of infected branches, chemical control of vectors, and/or rouging of severely affected plants) are expensive, ineffective, or environmentally damaging.

Recent studies on various aspects of the epidemiology of CVC ([1], and references therein) have provided fundamental information which can be used to develop a cellular automata (CA) model of the pathosystem. CA or other epidemic models could become relevant tools for addressing numerous practical and experimental questions: forecasting the progress and final intensity of CVC, planning and evaluation of strategies for disease control, and determination of the relevant mechanisms involved in the disease spreading.

In this paper, we propose a simple CA model to simulate CVC progress in which some epidemiological and environmental features, such as vector motility, plant stress, and seasonal modulations, are included. The simulation results are compared with CVC progress curves in time and spatial infection patterns observed in the São Paulo region.

II. EXPERIMENTAL DATA ON CVC EPIDEMICS

A. CVC progress in time

The CVC epidemic was observed by visual assessments of typical symptoms occurring on leaves or fruits, in 11 groves of Pêra, Hamlin, and Natal sweet oranges cultivated in two farms of the northern areas (Bebedouro and Colina counties) of São Paulo state, Brazil. In such areas, severely attacked by CVC, are planted the more susceptible cultivars having the supposedly most propitious age for disease development. The field data were collected over a 20-month period, from September 1994 through March 1996. The CVC incidence was mapped bimonthly and the data for each area and each evaluation were transformed to a proportion of symptomatic plants for temporal characterization of the disease spread.

The CVC progress curves are shown, for four different groves, in Fig. 1. All of them are double sigmoid, which is a clear indication that CVC is a polycyclic disease characterized by the existence of two phases: one in which the disease spread is fast, contrasted with another in which the epidemic development is almost stopped. For each grove the observed

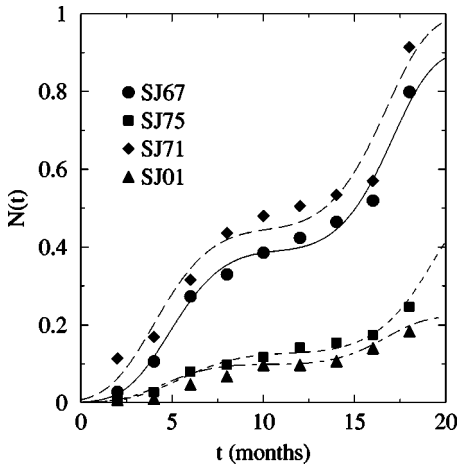

FIG. 1. Observed CVC progress curves in four groves SJ01, SJ67, SJ71, and SJ75. The curves represent generalized five-parameter logistic fittings to the observed data.

 ©2000 The American Physical Society

TABLE I. Coefficients of determination R^2 and estimated values of the five parameters describing the generalized logistic functions used to fit the observed data of CVC progress in four of the studied groves.

	Parameter					
Grove	p_1	p_2	p_3	p_4	p_5	R^2
SJ01	0.223	−6.000	1.647	−0.158	0.005	0.989
SJ67	0.908	−6.414	1.665	−0.153	0.005	0.996
SJ71	1.000	−4.854	1.307	−0.126	0.004	0.989
SJ75	0.526	−6.638	1.396	−0.120	0.004	0.993

data sets are fitted by five-parameter logistic curves [6] of the form

$$N(t)=\frac{p_1}{1+\exp[-(p_2+p_3t+p_4t^2+p_5t^3)]}. \tag{1}$$

Table I gives the corresponding parameters and the coefficients of determination (R^2) have been listed. In addition to the R^2 coefficient, the residual sums of squares for error and the consistency of the predicted values for the upper asymptotic fraction of diseased plants ($p_1 \leqslant 1$) were take into account to select the logistic among Gompertz and monomolecular generalized models with four or five parameters. It is important to note that sigmoid curves can be generated by different models (fitting equations). Indeed, the temporal increase of citrus tristeza virus, whose vectors are aphid species, follows a nonlinear Gompertz model [7].

B. Infected cluster size distribution functions

On any one of the orangeries containing about 10^3 trees there is no unique inoculum source. Each single infected plant or small initial group of infected plants grows by inoculating its adjacent neighbors, and aggregates with other affected trees, forming large clusters. As a result, the mean cluster size of infected trees increases in time and, in order to describe the disease spread, it is necessary to investigate the dynamic aspects of the distribution of infected plant aggregates generated by the CVC progress.

A cluster of diseased plants has been defined as any set of interconnected infected trees that are spatially isolated from any other group of diseased plants in the orangery. Then, the cluster size distribution function $n_s(t)$ is the fraction of these clusters consisting of s infected plants at time t, and was directly obtained by counting the number and size of diseased clusters present in the spatial patterns of the CVC epidemic, like those shown in Fig. 2, at each observation time.

Figure 3 shows the distribution $n_s(t)$ for one of the observed orangeries. It suggests that $n_s(t)$ follows a power-law distribution, that is, $n_s(t) \sim s^{-\alpha}$, over at least one decade of the argument s at any given time of CVC progress. A power-law distribution indicates the absence of a characteristic scale for the size of diseased plant aggregates. The exponents describing the power-law decay of $n_s(t)$ have values between 1.4 and 1.8 for all the orangeries studied. These values are characteristic of $1/f$ noise [23], as $1/f^{\gamma}$ spectra with γ in the interval [0,2] are commonly called. Therefore, the CVC infection dynamics has a $1/f$-like signal, which, from the physical point of view, is a sign of a cooperative phenomenon occurring in a spatially extended nonequilibrium system.

C. Self-affine profiles in CVC evolution patterns

Self-affine profiles [8,9] can be generated from the spatial patterns of diseased plants using various methods. The simplest of them is a 1:1 mapping between a given spatial configuration at time t, such as those shown in Fig. 2, and a ''walk process'' [10,11]. In this method each binary symbol $\sigma_i(t)$ describing the plant state [$\sigma_i(t)=0$: normal; $\sigma_i(t)=1$: diseased] is identified with a step (to the right or to the left) of a one-dimensional walk.

Specifically, to a unique spatial pattern $\{\sigma_1(t),\sigma_2(t),\ldots,\sigma_N(t)\}$ of N plants at fixed time t corresponds a profile given by the sequence of walker displacements h_i after i unit steps, $\{h_1(t),h_2(t),\ldots,h_N(t)\}$, defined as

$$h_i(t)=\sum_{j=1}^{i}\rho_j(t), \tag{2}$$

where $\rho_j=1$ if $\sigma_j=1$ (step to the right), or $\rho_j=-1$ if $\sigma_j=0$ (step to the left). Profiles generated at two distinct observation times in a given orangery using this walk process are shown in Fig. 4.

After obtaining the profiles by the walk process, we can investigate the nature of their correlations through analysis

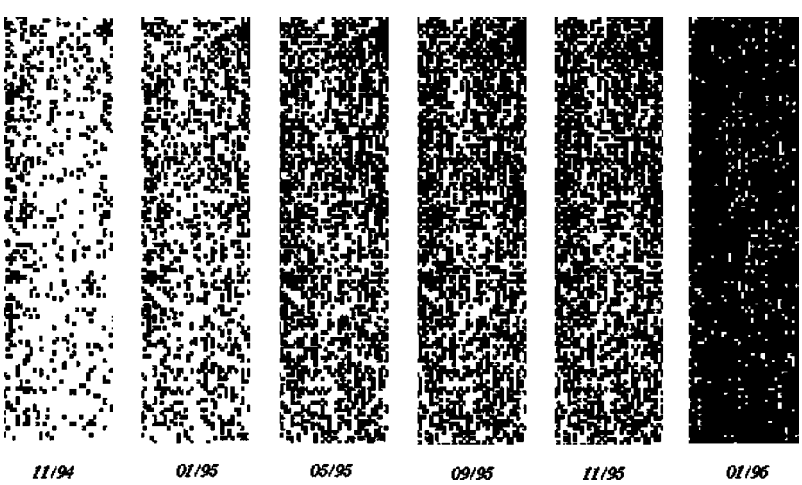

FIG. 2. Temporal sequence of CVC incidence maps in the grove SJ71 with 3960 Pêra orange trees. Six representative evaluations (11/94, 01/95, 05/95, 09/95, 11/95, and 01/96) are shown. Each black square corresponds to one symptomatic plant.

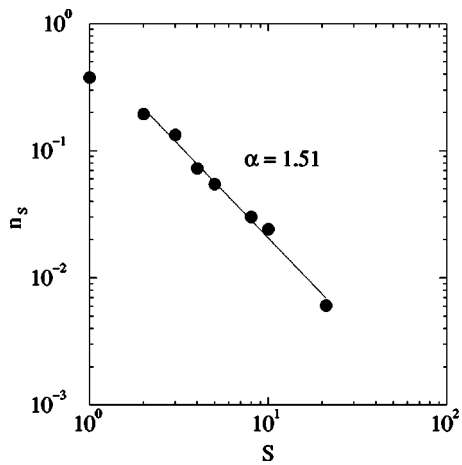

FIG. 3. Observed cluster size distribution function $n_s(t)$ of clusters containing s diseased plants for the grove SJ71 at the observation time $t=6$ months. The straight line represents the best fit to the data; its slope gives the exponent α describing the power-law decay of $n_s(t)$.

of the profile roughness [9]. The statistical measure W, which characterizes the roughness of the walk profile, is defined by the rms fluctuation in the displacement,

$$W(N,t)=\sqrt{\frac{1}{N}\sum_{i=1}^{N}[h_i(t)-\overline{h}(t)]^2}, \tag{3}$$

where

$$\overline{h}(t)=\frac{1}{N}\sum_{i=1}^{N}h_i(t) \tag{4}$$

is the mean displacement of the walk.

For self-affine profiles the roughness $W(N)$ will be described by a power-law scaling,

$$W(N)\sim N^H, \tag{5}$$

with the exponent H restricted to the interval [0,1] and related to the fractal dimension of the profile [8]. $H=1/2$ corresponds to a random walk; $H>1/2$ implies that the profile presents persistent correlations, and profiles with $H<1/2$ are anticorrelated.

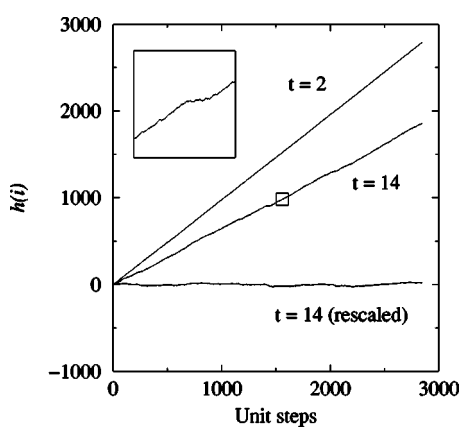

FIG. 4. Self-affine profiles generated by the walk process method at two distinct observation times in the grove SJ75, containing 2880 Pêra orange plants. The rescaled profile at $t=14$ months was obtained by subtracting the corresponding linear fitting of the data. The inset is an enlargement of the central region of the profile at $t=14$.

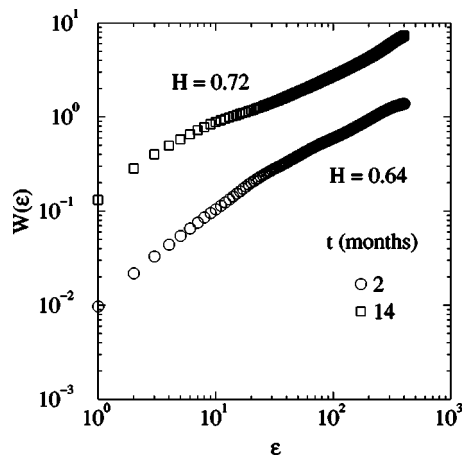

FIG. 5. Typical log-log plot of $W(\epsilon)$ versus ϵ used to calculate the roughness or Hurst exponent characterizing a rough profile, in this case the CVC spatial patterns in grove SJ75 at two distinct observation times. The Hurst exponent corresponds to the slope of the straight line fitting the linear part of the curve.

As one can see in Fig. 4, the profiles generated from the CVC epidemic patterns usually have drift. This is the reason that we use the method of roughness around the rms straight line [12] to evaluate the Hurst exponent H. In this method the roughness $W(N,\epsilon)$ on the scale ϵ is given by

$$W(N,\epsilon)=\frac{1}{N}\sum_{i=1}^{N}w_i(\epsilon) \tag{6}$$

and the local roughness $w_i(\epsilon)$ is defined as

$$w_i(\epsilon)=\sqrt{\frac{1}{2\epsilon+1}\sum_{j=i-\epsilon}^{i+\epsilon}\{h_j-[a_i(\epsilon)x_j+b_i(\epsilon)]\}^2}. \tag{7}$$

$a_i(\epsilon)$ and $b_i(\epsilon)$ are the linear fitting coefficients to the displacement data in the interval $[i-\epsilon,i+\epsilon]$ centered on the site i. Again, self-affine profiles satisfy the scaling law

$$W(\epsilon)\sim\epsilon^H. \tag{8}$$

The method described here was used to characterize the spatio-temporal patterns generated by elementary one-dimensional deterministic cellular automata [13].

A typical log-log plot of $W(\epsilon)$ versus ϵ used to calculate the Hurst exponent is shown in Fig. 5. This exponent characterizes the spatial patterns generated by a CVC epidemic. For all the analyzed orangeries the profiles are self-affine with Hurst exponents markedly different from 1/2, which means that long-range correlations present in the spatial disease patterns. Also, the roughness exponent increases from an initial value around 1/2, indicating a random infection pattern at the beginning, toward its maximum value 1, which corresponds to a totally infected orangery. Thus our results show that a CVC epidemic gives rise to aggregated patterns in which the inoculum level tends to be high in scattered sequences of neighboring plants, i.e., infected plants tend to be close to other diseased trees and the same holds for nor-

mal plants. Therefore, it appears that the pathogen occurs in small clusters which progressively expand by a contagion process mediated by vectors that predominantly spread from plant to plant.

III. A CELLULAR AUTOMATA MODEL FOR CVC

Stochastic CA models have been used before in plant pathology to simulate diseases spreading through spore dispersal [16], the infection dynamics of *R. Solani* [17], and the infection of cereal roots by the take-all fungus [18,19], but traditionally the mathematical modeling of plant disease is based on systems of differential equations [19].

CAs are totally discrete dynamical systems (discrete space, discrete time, and discrete number of states) which provide simple models for a great number of problems in science [14,15]. With each site (denoted i) is associated a variable σ_i, which can be in K different states $\sigma_i = 0,1,\ldots,K-1$. The dynamics is defined, at each time step, by rules depending on the values at previous times of $\{\sigma_i\}$ associated with a given number of q arbitrary sites (called inputs). Usually one considers regular lattices and the inputs refer to the sites in the local neighborhood only. The local rules of a CA may be probabilistic or deterministic and the sites are simultaneously updated.

In order to design the CA model for CVC spreading, we take into account the following basic features of the CVC pathosystem characterized in the previous section. The bacterium *X. fastidiosa* is transmitted by sharpshooter vectors of rather limited motility in the groves. This hypothesis is consistent with the results obtained for the roughness or Hurst exponents describing the CVC infection patterns. In diseased plants, the bacterium is systemic; nutritional imbalance and general weakness are commonly observed. Thus, the infected sites continuously act as inoculum sources to other healthy plants. Since there has been no measured effect of wind direction or machine based cultural practices on CVC spreading [1], the vector flies were assumed to be completely random in our model. Also, in healthy stressed trees the observed sharpshooter population is small, since these insects are preferably attracted by plants with new vegetative growth. Finally, as shown by the CVC progress curves, seasonal effects play a central role in disease spreading. In fact, the fastest CVC spreading progress is observed from September/October (flowering) through March (end of summer), a period associated with high temperatures, regular rains, and vegetative growth. The seasonal modulations are included in the CA model through variation in the motility of sharpshooter vectors as well as in the fraction of normal plants under hydric and nutritional stress. The functional form assumed to model such seasonal variations in our model is a sine wave function.

In our CA model the orangery is represented by square lattices of linear size L with null fixed boundary conditions (isolated grove, i.e., all the state variables are zero outside the lattice). The state of each plant is described by two binary variables $\sigma_{i,j}^{(1)}$ and $\sigma_{i,j}^{(2)}$, where $i,j=1,2,\ldots,L$. $\sigma_{i,j}^{(1)}=0$ represents a healthy (normal) plant and $\sigma_{i,j}^{(1)}=1$ a diseased plant, whereas $\sigma_{i,j}^{(2)}=1$ represents a plant under hydric or nutritional stress and $\sigma_{i,j}^{(2)}=0$ a nonstressed plant. Finally, the fraction of inoculative vectors at each site is also represented by a binary variable $\tau_{i,j}$. $\tau_{i,j}=0$ means a low fraction of inoculative sharpshooter leafhoppers in the insect population and $\tau_{i,j}=1$ a high inoculative fraction.

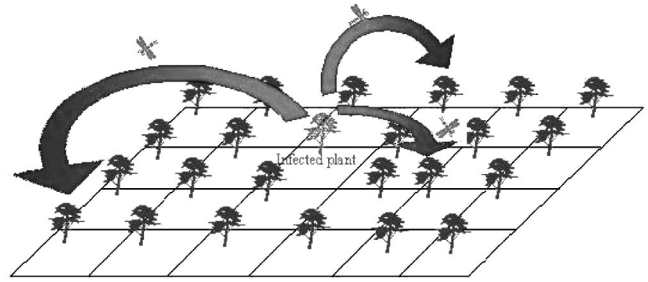

FIG. 6. Schematic representation of CVC spreading from a diseased plant (central gray square) used in our CA model. The central infected site acts as an inoculum source for $n_v(t)=3$ other distinct sites whose distances r are chosen from a symmetric Lévy distribution. These ''target'' sites are reached through the vector flies represented by the arrows. $n_v(t)$ changes seasonally with time.

In all simulations, random initial conditions have been used in which any plant of the lattice is diseased with probability p_{inf}, and stressed with probability $p_{st}(0)$. Since CVC causes severe stress in a diseased plant [1], an infected tree $(\sigma_{i,j}^{(1)}=1)$ immediately becomes stressed $(\sigma_{i,j}^{(2)}=1)$ in our model.

All the sites are simultaneously updated using the following local rules.

(i) For an infected site the corresponding state at the next time step is $\sigma_{i,j}^{(1)}=1$, $\sigma_{i,j}^{(2)}=1$ (diseased and stressed tree), and $\tau_{i,j}=1$ (high fraction of inoculative vectors). In addition, as shown in Fig. 6, each infected site acts as an inoculum source for $n_v(t)$ distinct plants at distance r_k, $k=1,2,\ldots,n_v$, chosen at random according to a symmetric Lévy distribution

$$p(r)=\frac{1}{2\pi}\int_{-\infty}^{+\infty} dt\, \exp[it(\mu-r)-|t|^a]. \tag{9}$$

Thus, the lengths of each of the $n_v(t)$ vector flights are not constant but rather are chosen from a probability distribution with a power-law tail. Each one of these selected neighbors will assume, at the next time step, the state $\sigma_{i,j}^{(1)}=1$, $\sigma_{i,j}^{(2)}=1$, and $\tau_{i,j}=1$, if it is a normal and nonstressed plant. Otherwise, the selected neighbor will stay in the same state as previously. Thus, in our CA model a healthy stressed tree is not infected by CVC, since the main vectors (*D. costalimai* and *Acrogonia* spp.) are preferentially observed in plants exhibiting young buds and leaves. In contrast, a healthy and nonstressed plant becomes diseased if it is reached by inoculative vectors coming from at least one infected site.

(ii) For a normal (stressed or nonstressed) plant not a target of a given diseased plant, the corresponding state at the next time step is $\sigma_{i,j}^{(1)}=0$ (normal) and $\tau_{i,j}=0$ (low fraction of inoculative vectors). Yet the value of $\sigma_{i,j}^{(2)}=0$ or 1 is chosen at random with probability $p_{st}\equiv 1-p_{nst}(t)$.

(iii) In order to simulate the seasonal effects on both plant stress and vector motility, the number of inoculative vector flights $n_v(t)$ and the probability associated with a nonstressed plant $p_{nst}(t)$ are periodic functions of time given by

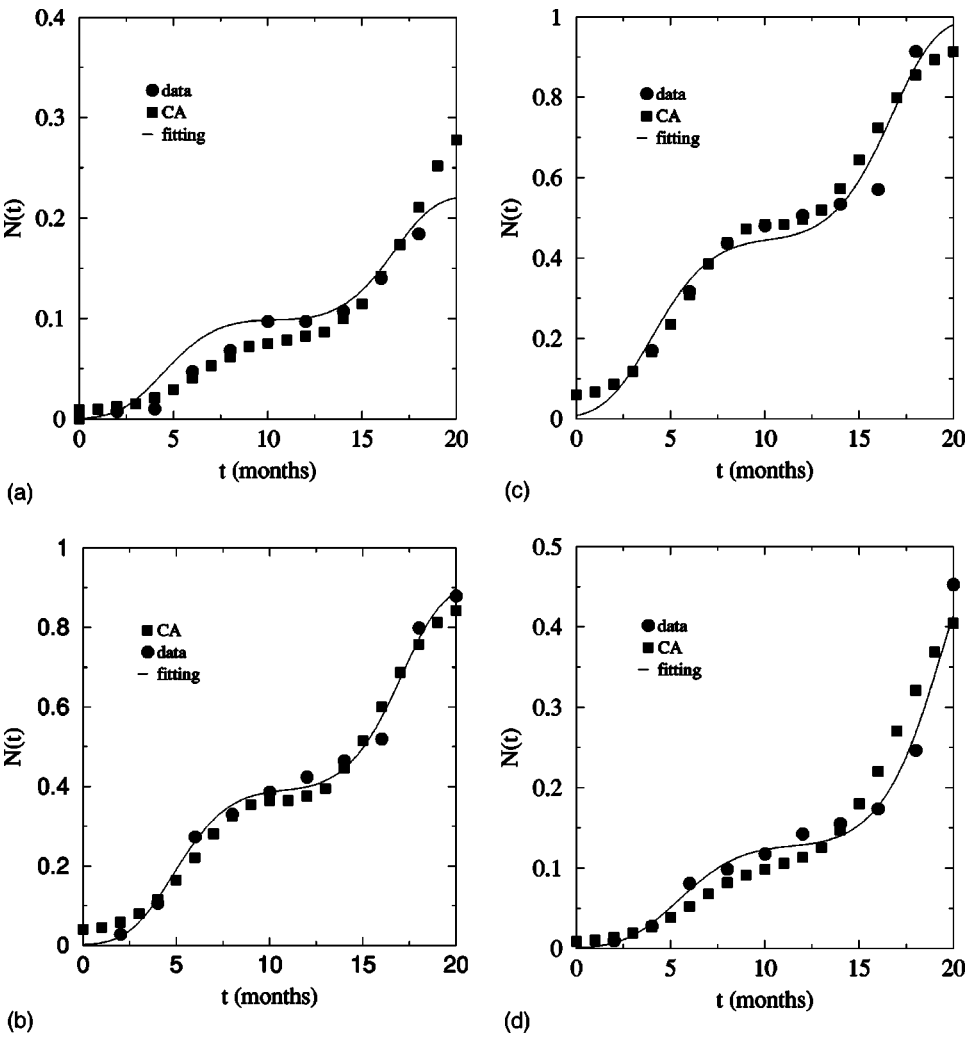

FIG. 7. Comparison between the CA generated and fitted CVC progress curves for groves (a) SJ01, (b) SJ67, (c) SJ71, and (d) SJ75. The observed data are also shown, and the CA parameters used are those listed in Table II. The data correspond to an average over 100 different realizations of CA evolution. The error bars are equal to or smaller than the symbol size.

$$n_v(t)=n_0+\mathrm{INT}\left[n_0\sin\left(\frac{2\pi t}{T}+\phi\right)\right], \tag{10}$$

$$p_{nst}(t)=p_{min}+(1-2p_{min})\times\frac{1+\sin(2\pi t/T+\phi)}{2}, \tag{11}$$

where INT means the integer part, n_0 is the time averaged number of inoculative vector flights, p_{min} is the minimum probability of finding a nonstressed plant, and T is the period of one year. ϕ is a common phase angle to describe possible time shifts between the simulated and field data.

Finally, we shall discuss some simplifications of our CA model for CVC progress. The use of a symmetric periodic function to model the seasonal effects should be thought of as a rough approximation to the much more complex climatic variations observed in nature. Another simplification is that once infected a given plant immediately acts as an inoculum source, in contrast to the classical notion of a discontinuous infectious period. It is known that the spread of disease involves the interplay of two dynamical processes: the mechanisms of transmission and the evolution of the pathogen within hosts. The basic questions of how the bacteria spread within the xylem system and what is the mechanism of pathogenesis in CVC are unanswered. In particular, it seems that the CVC symptoms in plants depend on the rate and extent of colonization by the bacteria. Also, a recent study [20] shows that efficient transmission of *X. fastidiosa* by vectors occurs only after its population overcomes a threshold in plant hosts. In addition, the transmission rate increases as the bacterial population in a plant increases. These features are not included in our CA model due to the lack of information about the system of *X. fastidiosa* in citrus.

IV. RESULTS

Now we shall report on the simulation results for our CA model. In all simulations a linear size $L=200$, a seasonal period $T=12$ months (one year), and a phase angle $\phi=-60°$ (a shift of two months between the observed and simulation initial times) were used. The remaining five CA parameters, namely, n_0, p_{inf}, p_{min}, μ, and a, were varied in order to compare the simulated and observed CVC progress curves. The results for four groves are shown in Fig. 7. As one can see, the CA progress curves show qualitatively the same functional behavior as the measured curves. A surprisingly quantitative agreement between the CA and the observed CVC progress curves was even obtained. The CA parameter values are listed in Table II. Therefore our simulation results suggest that the Lévy distribution of vector flights is universal, with $\mu=4$ and $a=0.68$. The same holds true for n_0, the time averaged number of sharpshooter vector

TABLE II. CA parameters used to simulate CVC progress curves corresponding to the observed data for four groves.

	Parameter				
Grove	μ	a	n_0	p_{inf}	p_{min}
SJ01	4	0.68	5	0.0002	0.001
SJ67	4	0.68	5	0.04	0
SJ71	4	0.68	5	0.06	0.35
SJ75	4	0.68	5	0.009	0

flies starting from each infected plant, which assumed a value 5 for all four simulated groves.

At this point, it is interesting to note that our CA model even predicts triple, quadruple, or greater sigmoid progress curves depending on the time elapsed up to a total infection of the grove. This simulation prediction can easily be tested simply by observing the CVC progress in the field for a period greater than 20 months as was done in the present work. Moreover, such triple or quadruple sigmoid curves can be mathematically modeled by using generalized logistic, monomolecular, or Gompertz functions only if the disease progress curves are subdivided into three or four parts that are analyzed separately. However, this approach is inadequate to describe the entire disease dynamics and to determine several parameters of epidemiological importance [21,22].

Figure 8 shows a simulated temporal sequence of CVC incidence maps qualitatively similar to the observed spatial patterns of CVC (see Fig. 2). From such incidence maps, one can determine the dynamic infected cluster size distribution function $n_s(t)$ and the roughness exponent H characterizing the self-affinity of CVC infection profiles. Figures 9 and 10 show, respectively, the cluster size distribution function $n_s(t)$ and typical log-log plots of $W(\epsilon)$ versus ϵ corresponding to the simulated infection maps for the grove SJ71 at various observation times. Both the power-law decay of the infected cluster size distribution function and the roughness exponents characterizing the spatial disease patterns indicate the presence of long-range correlations in CVC development. Roughness exponents greater than 1/2 mean that in the neighborhood of a diseased plant the probability of finding another infected tree increases. A significant aggregation of diseased plants suggests that the pathogen predominantly spreads from plant to plant. Since our CA model permits fast simulations of many large samples of artificial CVC pathosystems in various epidemiological contexts, the numerical values for the exponents α and H can be determined with a reliable statistical precision difficult to attain in actual field observations.

It is important to emphasize that a simple random walk distribution for the inoculative vector flights constrained to a local neighborhood of radius $r(t)$ around each diseased plant also generates progress curves in good agreement with the field data. However, the resulting CVC incidence maps are clearly different from those observed. Random flights of inoculative vectors produce spots of diseased plants artificially isolated in space, which grow to merge with other infected clusters. In contrast, a Lévy distribution permits rare long-range vector flights, which appears to be an essential feature in explaining the scale invariance observed in CVC spread. Indeed, conventional random walks used to model foraging behavior in biology [24] predict a Poisson instead of a scale-invariant power-law distribution. Thus, our results suggest that the inoculative sharpshooter leafhoppers ($\sim$1 cm in size) perform long flights of random foraging, searching for nonstressed plants with new vegetative growth unpredictably dispersed over several square kilometers. A possible explanation is that, for insects operating in swarms or flocks comprised of N walkers, Lévy flight search patterns (for which Nt sites are visited after t steps) are much more efficient than Brownian walk foraging patterns [for which only $t ln(N/lnt)$ distinct sites are visited] [25]. It is interesting that Lévy flight search strategies are also observed in albatrosses [26].

V. CONCLUSIONS

In this study a spatio-temporal analysis of CVC spread was carried out. The shape of the observed CVC progress curves was double sigmoid, best fitted by a five-parameter generalized logistic function. This means that CVC is a polycyclic disease in which a phase of rapid progress alternates with another of almost no change. In addition, both the power-law decay of the infected cluster size distribution functions and the roughness exponents characterizing the spatial disease patterns indicate the presence of long-range correlations in CVC development.

In order to understand the basic mechanisms by which the features discussed above emerge, a CA model was proposed. It takes into account the motility of sharpshooter vectors, the

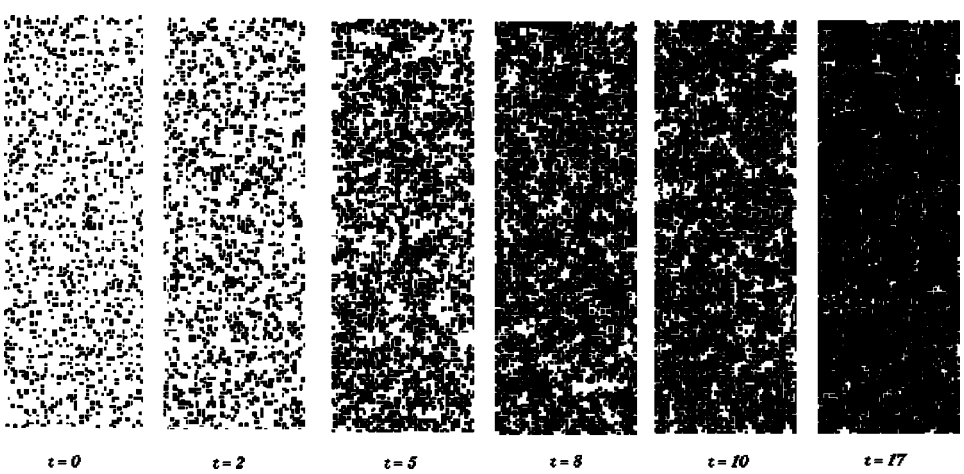

FIG. 8. A simulated sequence of CVC incidence maps in the grove SJ71. Each black square corresponds to one symptomatic plant.

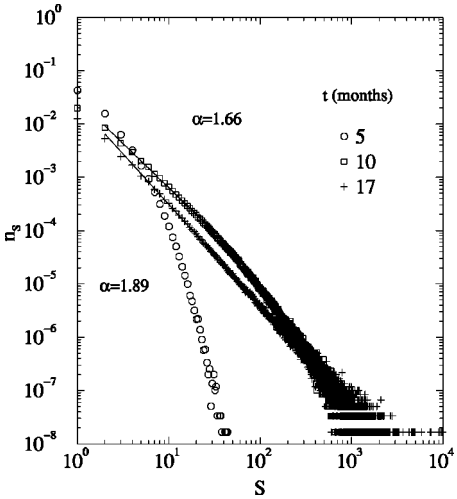

FIG. 9. Simulated cluster size distribution function $n_s(t)$ for the grove SJ71 at various observation times. The straight line represents the best fit to the data; its slope gives the exponent α describing the power-law decay of $n_s(t)$. The data correspond to an average over 100 different realizations of CA evolution.

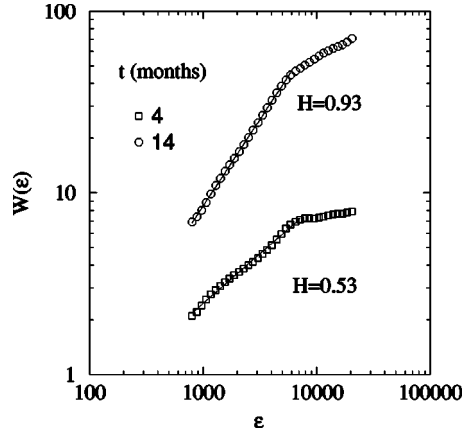

FIG. 10. Typical log-log plot of $W(\epsilon)$ versus ϵ corresponding to the simulated infection profiles for the grove SJ71 at two observation times. The straight line represents the best fit to the data; its slope gives the roughness exponent H describing the profile. The data correspond to an average over 20 different realizations of CA evolution.

level of plant hydric and nutritional stress, and seasonal climatic effects. By varying the CA parameters controlling these factors, a good agreement between the simulation and all the observed data was achieved, suggesting that the actual relevant mechanisms of CVC spreading were really captured and evidenced by the evolution rules of the proposed CA model. Therefore, our model suggests that the average number $n_v(t)$ of Lévy flights performed by the sharpshooter vectors as well as plant stress, described by the probability p_{st}, are the most fundamental parameters determining the aspects of CVC spreading. These factors are also affected by seasonal variations.

ACKNOWLEDGMENTS

This work was partially supported by FAPEMIG and CNPq, Brazilian agencies.

[1] F. F. Laranjeira, MS dissertation, Universidade de São Paulo, ESALQ, Piracicaba, Brazil, 1997 (unpublished).
[2] D. A. Palazzo and M. L. V. Carvalho, Laranja, Cordeirópolis **13**, 489 (1992).
[3] M. J. G. Beretta, R. C. S. Coelho, A. M. B. Leal, T. T. Gama, R. F. Lee, and K. S. Derrick, Fitopatol. Bras. **18**, (supplement) 277 (1993).
[4] J. R. S. Lopes, M. J. G. Beretta, R. Harakava, R. P. P. Almeida, R. Krügner, and A. Garcia Jr., Fitopatol. Bras. **21** (suplemento), 343 (1996).
[5] S. R. Roberto, A. Coutinho, V. S. Miranda, and J. E. O. Lima, Fitopatol. Bras. **20** (supplement), 348 (1995).
[6] B. Hau, L. Amorim, and A. Bergamin Filho, Phytopathology **83**, 928 (1993).
[7] T. R. Gottwald, S. M. Garnsey, and J. Borbón, Phytopathology **88**, 621 (1998).
[8] T. Vicsek, *Fractal Growth Phenomena*, 2nd ed. (World Scientific, Singapore, 1992).
[9] A. L. Barabási and H. E. Stanley, *Fractal Concepts in Surface Growth* (Cambridge University Press, Cambridge, England, 1995).
[10] C. K. Peng, S. V. Buldyrev, A. L. Goldberger, S. Havlin, F. Sciortino, M. Simons, and H. E. Stanley, Nature (London) **356**, 168 (1992).
[11] H. E. Stanley, S. V. Buldyrev, A. L. Goldberger, Z. D. Goldberger, S. Havlin, R. N. Mantegna, S. M. Ossadnik, C. K. Peng, and M. Simons, Physica A **205**, 214 (1994).
[12] J. G. Moreira, J. Kamphorst Leal da Silva, and S. Oliffson Kamphorst, J. Phys. A **27**, 8079 (1994).
[13] J. A. Sales, M. L. Martins, and J. G. Moreira, Physica A **245**, 461 (1997).
[14] S. Wolfram, *Theory and Applications of Cellular Automata* (World Scientific, Singapore, 1986).
[15] G. B. Ermentrout and L. Edelstein-Keshet, J. Theor. Biol. **160**, 97 (1993).
[16] K. P. Minogue and W. E. Fry, Phytopathology **73**, 1168 (1983).
[17] A. Kleczkowski, C. A. Gilligan, and D. J. Bailey, Proc. R. Soc. London Ser. B **264**, 979 (1997).
[18] C. A. Gilligan, New Phytol. **128**, 539 (1994).
[19] C. A. Gilligan, Can. J. of Plant Pathol. **17**, 96 (1995).
[20] B. L. Hill and A. H. Purcell, Phytopathology **87**, 1197 (1997).
[21] L. Amorim and A. Bergamin Filho, Z. Pflanzenk. Pflanzenschutz **98**, 605 (1991).
[22] L. Amorim, A. Bergamin Filho, and B. Hau, Phytopathology **83**, 933 (1993).
[23] P. Bak, C. Tang, and K. Wiesenfeld, Phys. Rev. Lett. **59**, 381 (1987).
[24] H. C. Berg, *Random Walks in Biology* (Princeton University Press, Princeton, 1983), p. 81.
[25] H. Larralde, P. Trunfio, S. Havlin, H. E. Stanley, and G. H. Weiss, Nature (London) **355**, 423 (1992).
[26] G. M. Viswanathan, V. Afanasyev, S. V. Buldyrev, E. J. Murphy, P. A. Prince, and H. E. Stanley, Nature (London) **381**, 413 (1996).